Jet production and studies of nucleon/nuclear PDFs

R. Vogt

Physics Division, Lawrence Livermore National Laboratory, Livermore, CA 94551, USA

Physics Department, University of California, Davis, CA 95616, USA

‘Recent’ Parameterizations of Nuclear Parton Densities

EKS98: K. J. Eskola, V. J. Kolhinen and P. V. Ruuskanen, Nucl. Phys. B 535 (1998) 351 [arXiv:hep-ph/9802350]; K. J. Eskola, V. J. Kolhinen and C. A. Salgado, Eur. Phys. J. C 9 (1999) 61 [arXiv:hep-ph/9807297].

EPS09: K. J. Eskola, H. Paukkunen and C. A. Salgado, JHEP 0904 (2009) 065 [arXiv:0902.4154 [hep-ph]].

nDS: D. de Florian and R. Sassot, Phys. Rev. D 69, 074028 (2004) [arXiv:hep-ph/0311227].

DSSZ: D. de Florian, R. Sassot, M. Stratmann and P. Zurita, Phys. Rev. D 85, 074028 (2012) [arXiv:1112.6324 [hep-ph]].

HKN: M. Hirai, S. Kumano and T. H. Nagai, Phys. Rev. C 70, 044905 (2004) [arXiv:hep-ph/0404093].

FGS10: L. Frankfurt, V. Guzey and M. Strikman, Phys. Rept. 512, 255 (2012) [arXiv:1106.2091 [hep-ph]].

EPS09s: I. Helenius, K. J. Eskola, H. Honkanen and C. A. Salgado, JHEP 1207, 073 (2012) [arXiv:1205.5359 [hep-ph]].

How Are They Similar?

Most determine the nuclear modifications to the parton densities (nPDFs) using methods similar to those used to fix the free proton parton densities

Some subset of the total available data is chosen to use in a global analysis: the lower the starting scale, the more prior data can be included since fixed-target data reached low x only at low Q^2

The behavior of the nPDFs at the starting scale Q_0^2 is parameterized as a function of x and A and subsequently evolved in Q^2 assuming collinear factorization and DGLAP evolution

The spatial dependence is usually not included, the global analysis only applies to averages over the whole nuclear volume

So far no LHC data are included in these analyses

Only the FGS sets deviate from this path – they relate the nuclear parton densities to the diffractive nucleon parton densities, their method allows natural inclusion of the spatial dependence

How Are They Different?

While there are a number of similarities in the various approaches, there are also differences

Differences include:

- **starting scale Q_0^2**
- **which data sets are used and how many points**
  - **a greater number of points from a given fixed-target data set can be used if $Q_0^2 = 1$ GeV^2 (DSSZ) than if $Q_0^2 = 4$ GeV^2 (FGS10)**
  - **neutrino (charged current) DIS is typically not used in global fits (DSSZ uses them)**
- **initial shape parameterization with x (is there antishadowing assumed and, if so, for which distributions?) and the minimum x allowed**
- **whether the treatment is to leading or next-to-leading order**
- **which proton parton densities are used for the baseline in ratios of the nuclear modifications**

LO and NLO nPDFs Should Give The Same Result

The nDS LO and NLO nuclear modifications for π^0 production at RHIC agree
This should be the case if the extractions are consistent order by order

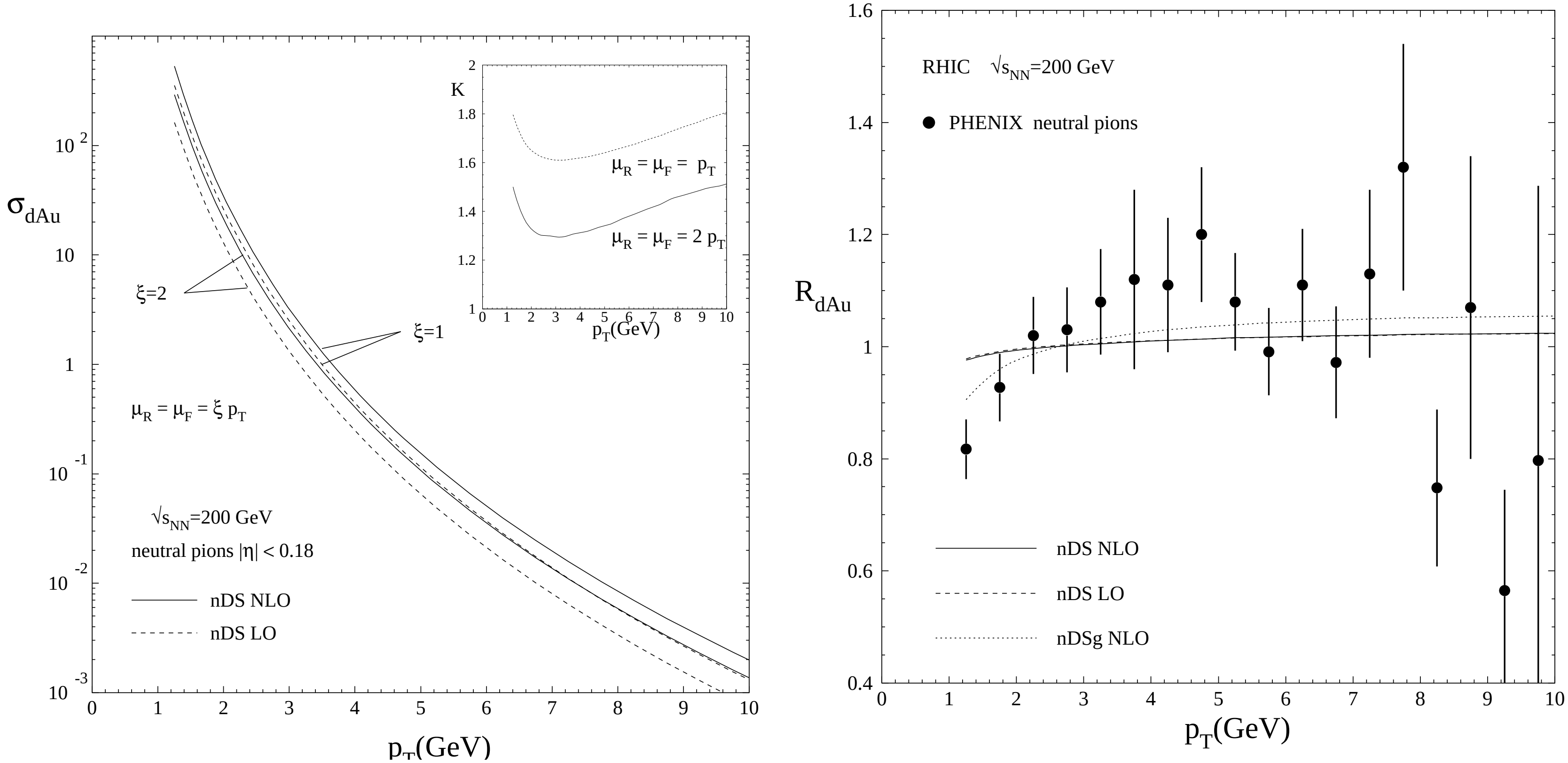

Figure 1: **Left: The π^0 cross section in d+Au collisions at $\sqrt{s_{NN}} = 200$ GeV at LO and NLO. Right: The LO and NLO calculations of $R_{\rm dAu}$.**

Comparison of FGS10 and EPS09 Sets at LO and NLO

FGS10 ratios show stronger low x modifications at NLO than at LO which tends to plateau at low x

EPS09 uncertainty band (obtained by varying each of the 15 parameters within $\pm 1\sigma$) is broader for LO and shows stronger modifications at LO than at NLO

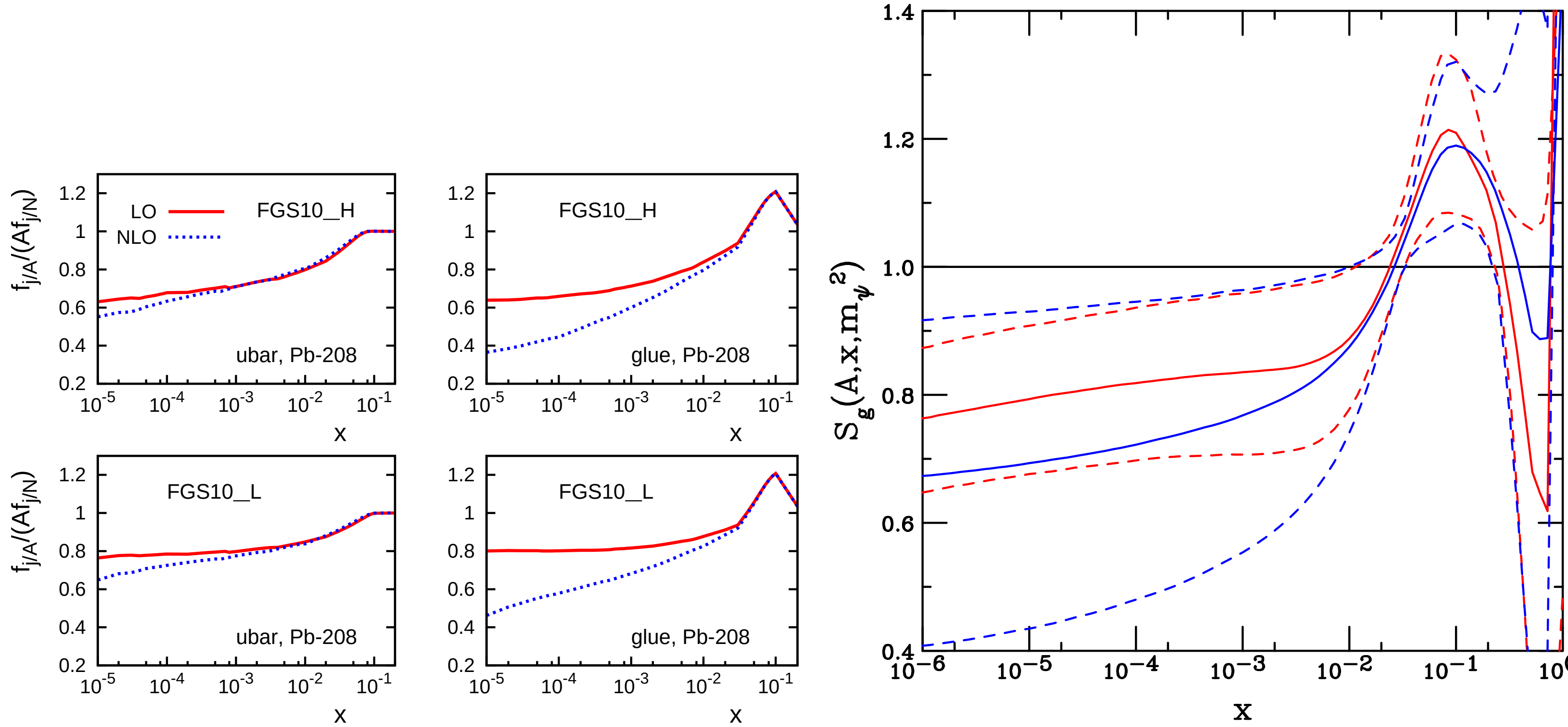

Figure 2: **Left: The difference between the FGS10_H (top) and FGS10_L (bottom) ratios LO and NLO for Q_0^2. Right: The difference between EPS09 LO (blue) and EPS09 NLO (red).**

Are The LO and NLO Derivations Consistent?

Probably Not...

J/ψ Hadroproduction at the LHC

In pp collisions, collinear factorization works very well, even for open charm and bottom production at low p_T

In collisions with nuclei, we are pushing the limits of some of the nPDFs, especially for forward production of quarkonium (ALICE and LHCb)

There has been only one p+Pb run at the LHC, $\sqrt{s_{_{NN}}} = 5$ TeV, similar to the expected top LHC Pb+Pb energy which will come soon

The LHC pA run helps open a new regime of low x and high Q^2 probes of the nPDFs (see Albacete *et al.*, Int. J. Mod. Phys. E 22 (2013) 1330007 [arXiv:1301.3395 [hep-ph]]

- Charged hadron $R_{p\mathrm{Pb}}$ up to $p_T \sim 200$ GeV from CMS and ATLAS, 30 GeV from ALICE
- Charged hadron $dN_{\mathrm{ch}}/d\eta$
- Forward (and backward) rapidity measurements of J/ψ, ψ' and Υ
- Rapidity distributions of Z^0, W^+ and W^-; lepton asymmetries for W^+/W^- production

R_{dAu} for J/ψ: LO vs NLO CEM

The x regions probed in the LO and NLO CEM are somewhat different because at LO in the total cross section, $p_T^{J/\psi} = 0$

However, the x regime is similar enough that if one calculates J/ψ at LO and NLO in the CEM with the same set of nPDFs (EKS98), the ratios are similar if not exactly the same

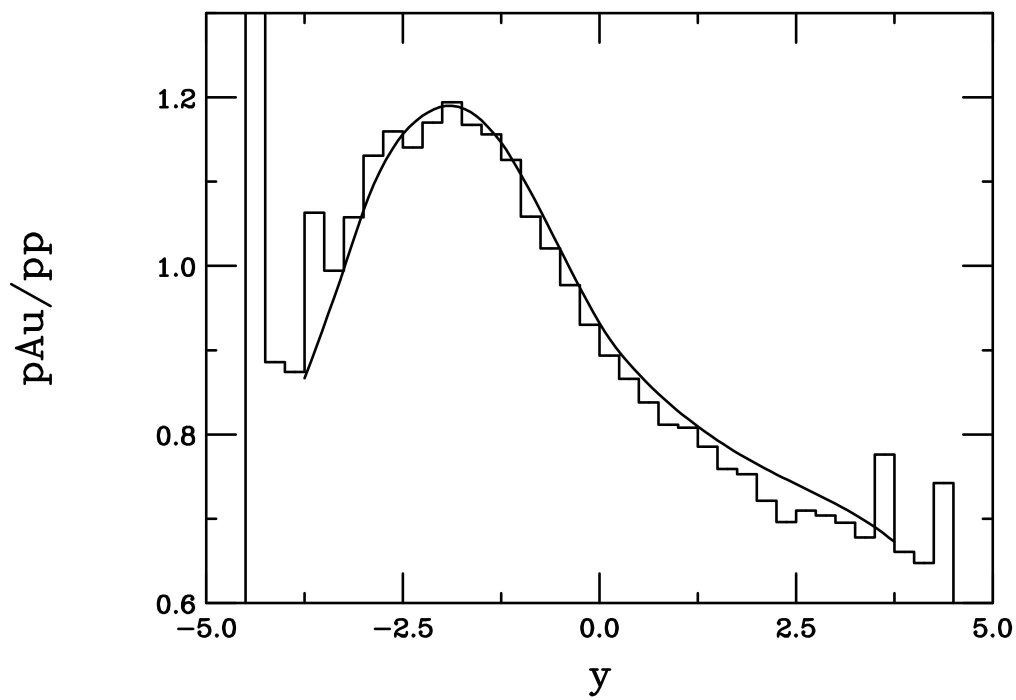

Figure 3: J/ψ **production in d+Au relative to** pp **as a function of rapidity for the LO (curve) and NLO (histogram) CEM at** $\sqrt{s_{NN}} = 200$ **GeV. Both calculations employ EKS98.**

$R_{p\mathrm{Pb}}$ for J/ψ: LO vs NLO CEM

Use EPS09 to compare the LO and NLO modifications in the CEM

Results do not agree, the stronger gluon modification of EPS09 LO is closer to the data while the EPS09 NLO sets underpredict the measured effect

LO band is larger due to greater uncertainty in EPS09 LO

Other effects (hadronic interactions, energy loss) may be important, J/ψ in hadroproduction is messy

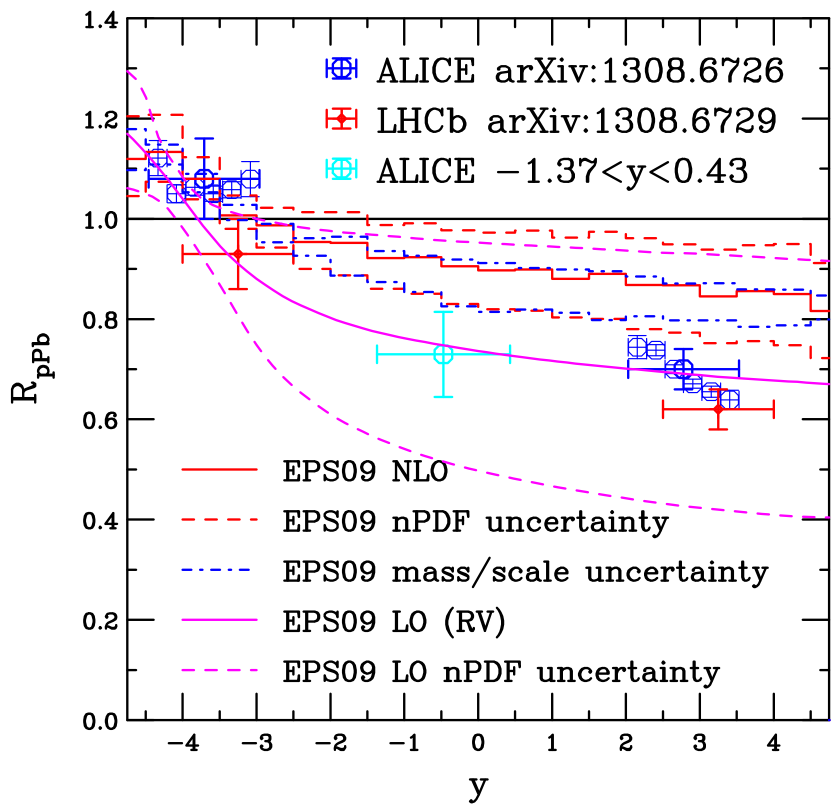

Figure 4: **The EPS09 LO calculations in the CEM (red) and CSM (cyan) are compared. The CEM calculation includes the full EPS09 uncertainty added in quadrature while the CSM calculation includes only the minimum and maximum uncertainty sets.**

J/ψ Production Mechanism is Small Effect: LO CEM vs LO CSM

There is some shift between the two central values, mostly due to the choice of mass and scale used in the calculation rather than overall kinematics (choosing a larger scale to make up for average p_T moves the CEM calculation closer)

CSM range obtained by taking the EPS09 sets with the biggest variation in the gluon nPDF, CEM uncertainty is calculated using all EPS09 LO sets and adding in quadrature

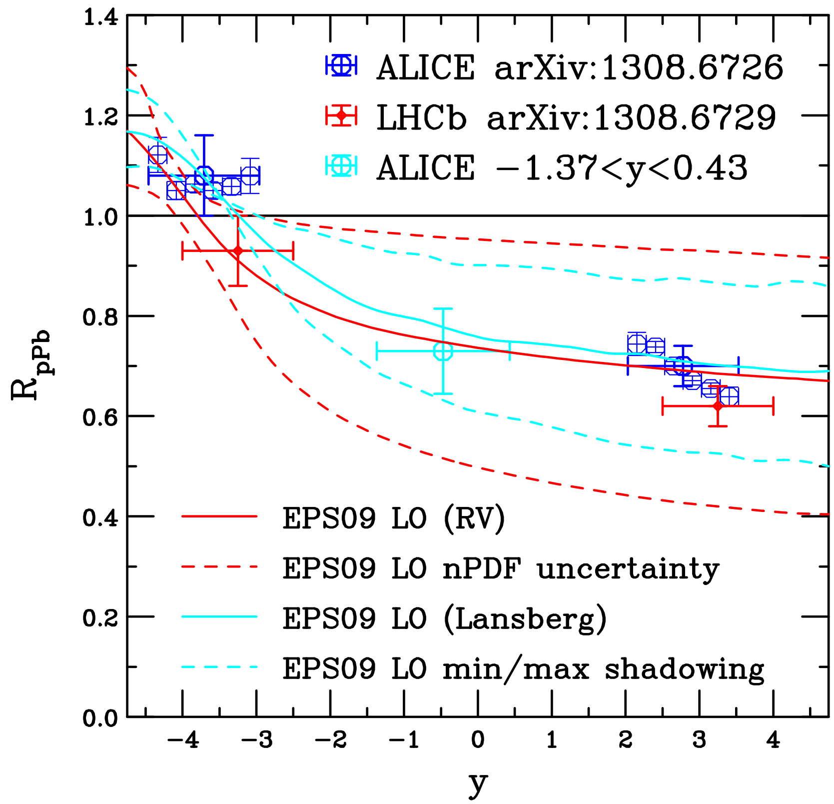

Figure 5: **The EPS09 LO calculations in the CEM (red) and CSM (cyan) are compared. The CEM calculation includes the full EPS09 uncertainty added in quadrature while the CSM calculation includes only the minimum and maximum uncertainty sets.**

UPCs are Cleaner Probes of nPDFs

Ultraperipheral collisions free of final-state effects as well as absorption

Very strong and very weak nPDFs can be ruled out

See Vadim's talk for analysis of these data relative to impulse approximation, an independent measure of gluon shadowing at low x, and evidence for significant shadowing

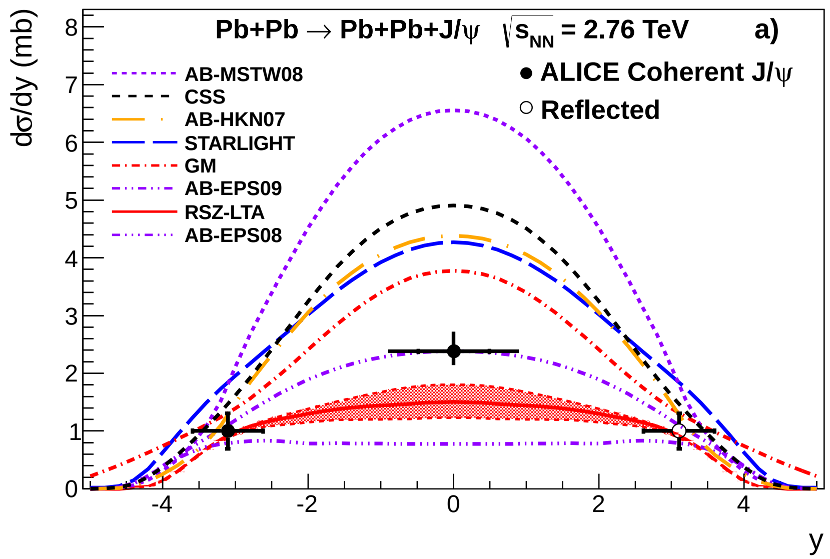

Figure 6: Coherent photoproduction of J/ψ in ultraperipheral Pb+Pb collisions at $\sqrt{s_{NN}} = 2.76$ TeV measured by ALICE in central and forward rapidities compared to various nPDF parameterizations. [From arXiv:1305.1467.]

Dijets and Heavy Flavor Jets in UPCs

Some time ago, Mark, Sebastian White and I calculated rates for dijet and b quark production in Pb+Pb and p+Pb interactions (PRL 96, 082001 (2006))

Idea was to explore the central region at relatively low x and high p_T

UPCs have an advantage over hadronic interactions because the high background in hadronic events is eliminated

We used a LO calculation with the MRST LO PDFs and no shadowing; assume minimum jet $p_T > 5$ GeV

ATLAS calorimeter acceptance was taken into account

We studied photon-gluon fusion only because the direct production dominates in these kinematics

We chose x_1 for the photon and x_2 for the gluon from the proton or the Pb nucleus
Rates are for a one month run at the top expected ion beam energy, 2.76 TeV, and top proton beam energy, 7 TeV, or $\sqrt{s_{NN}} = 5.5$ and 8.8 TeV respectively

Dijet Photoproduction in Pb+Pb UPCs

Event rates shown in bins of jet p_T as a function of $\log(x_2)$

The diagonals labeled E_γ indicate lines of constant photon energy: rates are dominated by $2.76 \leq E_\gamma \leq 110$ GeV

Measureable rates are obtained for $|y_{\rm jet}| \leq 3$

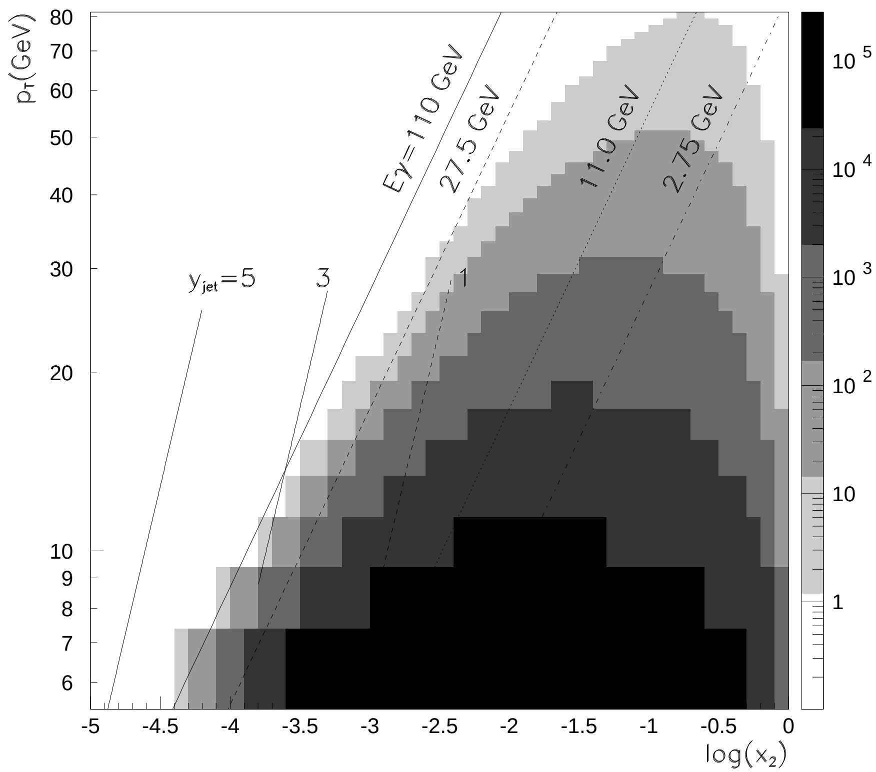

Figure 7: Inclusive dijet photoproduction rate in one month for the top Pb+Pb $\sqrt{s_{NN}}$ with a luminosity of 0.42×10^{27} cm^{-2}s^{-1}. The rates are in counts per bin of $\pm 0.25 x_2$ and ± 1 GeV in p_T.

Bottom Photoproduction in Pb+Pb and p+Pb UPCs

High p_T b jets measured with heavy flavor tag (soft lepton or secondary vertex)

The p_T reach is not as large as for dijets but rates are good

The higher energy of the p+Pb collisions broadens the available x range
Charm rates would be a factor of four or so higher

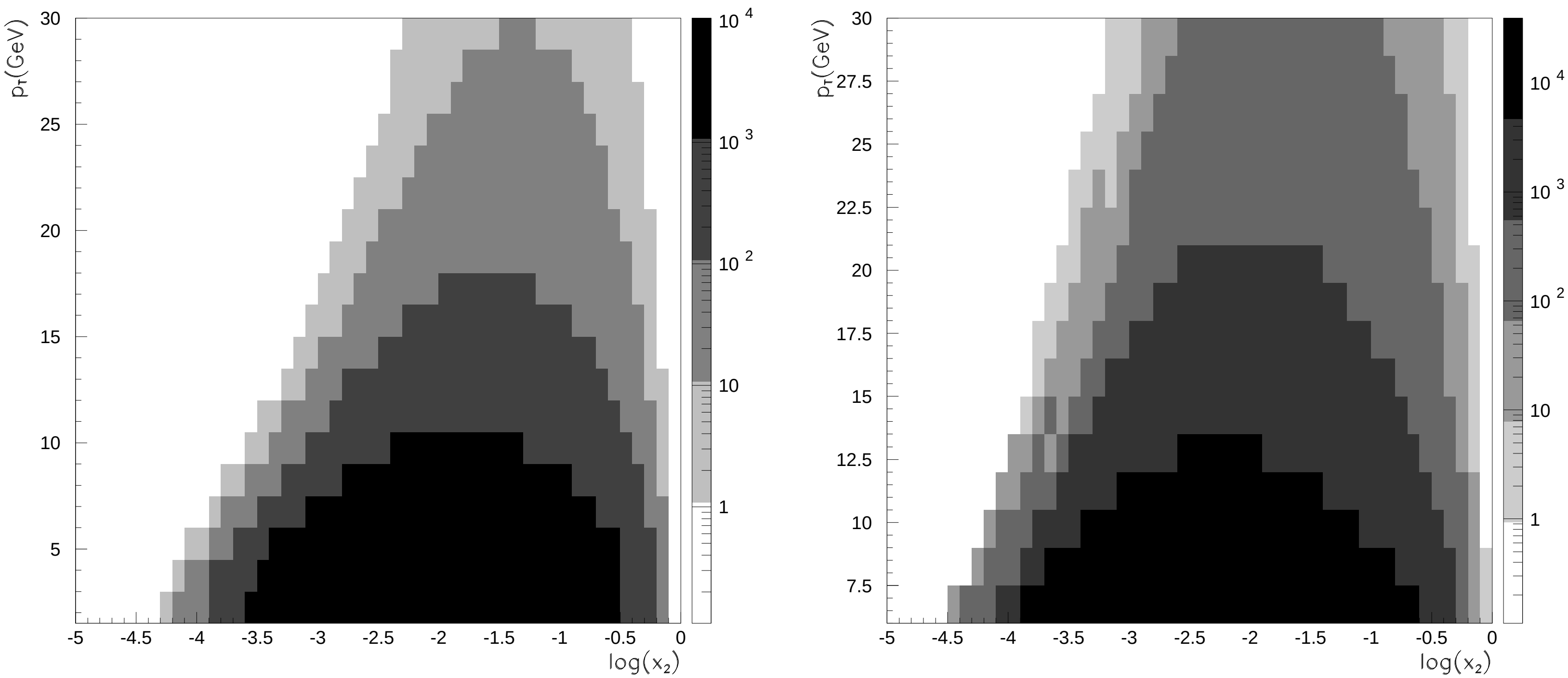

Figure 8: Inclusive $b\bar{b}$ photoproduction rate in one month for the top Pb+Pb $\sqrt{s_{NN}}$ with a luminosity of 0.42×10^{27} cm^{-2}s^{-1} (left) and top p+Pb energy with a luminosity of 7.4×10^{29} cm^{-2}s^{-1} (right). Note the linear scale for these results relative to the log p_T scale for dijets (previous). Note also the suppressed zero on the right-hand side. The rates are in counts per bin of $\pm 0.25 x_2$ and ± 0.75 GeV in p_T.

Summary

- Lots of nPDF parameterizations on the market, EPS09 is widely used
- Differences in LO and NLO results for EPS09 on J/ψ production illustrates the fact that gluon nPDF is still not very well constrained
- LHC p+Pb data could be taken into global analyses in the future
- UPC data could be important for these analyses, can study jet and heavy flavor production very cleanly, probing low x and moderate to high p_T simultaneously with little background
- If the LHC luminosities at full energy are higher than those we assumed, the rates would increase correspondingly
- For specifics on the various nPDF analyses, see the back up slides

Back Up Slides

Eskola *et al* Method I

Nuclear effects on PDFs divided into x regions

- shadowing; a depletion at $x \lesssim 0.1$,
- anti-shadowing; an excess at $0.1 \lesssim x \lesssim 0.3$,
- EMC effect; a depletion at $0.3 \lesssim x \lesssim 0.7$
- Fermi motion; an excess towards $x \to 1$ and beyond.

Define ratios of the individual and total valence and sea quark distributions and the gluon ratio in nuclei relative to protons

$$
\begin{aligned}
R_{\bar{q}}^{A}(x,Q^2) &\equiv \frac{\bar{q}_A(x,Q^2)}{\bar{q}(x,Q^2)} \quad R_{q_V}^{A}(x,Q^2) \equiv \frac{q_V^A(x,Q^2)}{q_V(x,Q^2)} \quad R_G^A(x,Q^2) \equiv \frac{g^A(x,Q^2)}{g(x,Q^2)} \\
R_V^A(x,Q^2) &\equiv \frac{u_V^A(x,Q^2)+d_V^A(x,Q^2)}{u_V(x,Q^2)+d_V(x,Q^2)}, \\
R_S^A(x,Q^2) &\equiv \frac{\bar{u}_A(x,Q^2)+\bar{d}_A(x,Q^2)+\bar{s}_A(x,Q^2)}{\bar{u}(x,Q^2)+\bar{d}(x,Q^2)+\bar{s}(x,Q^2)}
\end{aligned}
$$

Eskola *et al* Method II

Determination of $R_i^A(x,Q^2)$ from nuclear deep-inelastic scattering (nDIS) and Drell-Yan (DY) data

- Formulate $R_{F_2}^A(x,Q^2)$ and $R_{\mathrm{DY}}^A(x,Q^2)$ based on linear combinations of the quark and antiquark ratios
- Make an ansatz for $R_{F_2}^A(x,Q_0^2)$ based on nDIS data
- Decompose $R_{F_2}^A(x,Q_0^2)$ into R_V^A and R_S^A
- Constrain R_V^A using baryon number conservation
$\int_0^1 dx[u_V(x,Q_0^2)+d_V(x,Q_0^2)]R_V^A(x,Q_0^2) = \int_0^1 dx[u_V(x,Q_0^2)+d_V(x,Q_0^2)] = 3$
- Constrain $R_G^A(x,Q_0^2)$ by momentum conservation (gluons removed at low x get put back at higher x, for stability of R_V^A and R_S^A assume gluon EMC effect)
$1 = \int_0^1 dx\, x\Big\{g(x,Q_0^2)R_G^A(x,Q_0^2) + [u_V(x,Q_0^2)+d_V(x,Q_0^2)]R_V^A(x,Q_0^2) + 2[\bar{u}(x,Q_0^2)+\bar{d}(x,Q_0^2)+s(x,Q_0^2)]R_S^A(x,Q^2)\Big\}$
- Perform DGLAP evolution of the initial nPDFs which can further constrain gluon shadowing

$$\begin{aligned}\frac{\partial R_{F_2}^A(x,Q^2)}{\partial \log Q^2} &= \frac{\partial F_2^D(x,Q^2)/\partial \log Q^2}{F_2^D(x,Q^2)}\left\{\frac{\partial F_2^A(x,Q^2)/\partial \log Q^2}{\partial F_2^D(x,Q^2)/\partial \log Q^2} - R_{F_2}^A(x,Q^2)\right\}\\ &\approx \frac{5\alpha_s}{9\pi}\frac{xg(2x,Q^2)}{F_2^D(x,Q^2)}\left\{R_G^A(2x,Q^2) - R_{F_2}^A(x,Q^2)\right\}\end{aligned}$$

- Constrain $R_S^A(x,Q_0^2)$ and $R_V^A(x,Q_0^2)$ with Drell-Yan data
- Repeat, repeat, repeat

Eskola *et al* Parameterizations

Fits based on piecewize functions for $i = V, S$ and G

$$R_i^A(x) = \begin{cases} a_0 + (a_1 + a_2 x)[\exp(-x) - \exp(-x_a)] & x \leq x_a \\ b_0 + b_1 x + b_2 x^2 + b_3 x^3 & x_a \leq x \leq x_e \\ c_0 + (c_1 - c_2 x)(1 - x)^{-\beta} & x_e \leq x \leq 1, \end{cases}$$

y_0	**Height to which shadowing levels as $x \to 0$**
x_a, y_a	**Position and height of the antishadowing maximum**
x_e, y_e	**Position and height of the EMC minimum**
β	**Slope factor in the Fermi-motion part,**
$c_0 = 2y_e$	
$d_i^A = d_i^{A_C} \left(\frac{A}{A_C}\right)^{p_{d_i}}$	**A dependence of fit parameters follows power law relative to Carbo**

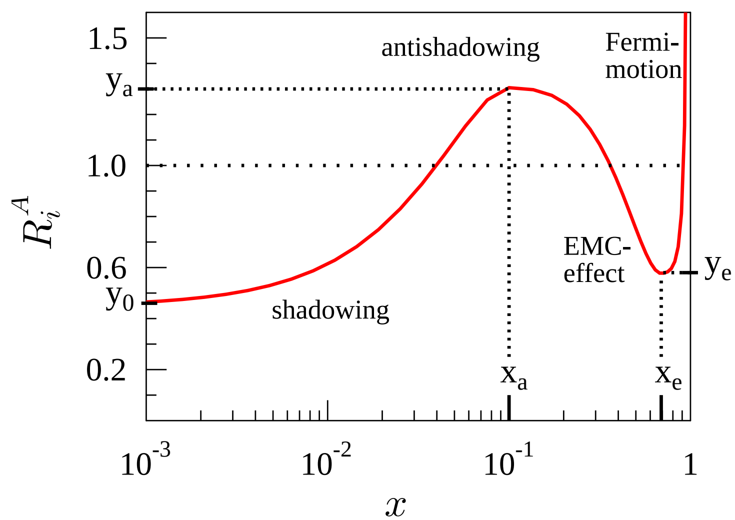

Figure 9: **An illustration of the fit function $R_i^A(x)$ and the role of the parameters x_a, x_e, y_0, y_a, and y_e.**

Differences Between Eskola *et al* Sets

EKS98 **Simple parameterization for all A; leading order analysis only; GRV LO set used for proton PDFs; single set; no χ^2 analysis performed; $2.25 \leq Q^2 \leq 10^4$ GeV^2; $10^{-6} < x < 1$**

EPS08 **Simple parameterization for all A; leading order analysis only; CTEQ61L set used for proton PDFs; single set; χ^2 analysis uses forward BRAHMS data from RHIC to maximize gluon shadowing; $1.69 \leq Q^2 \leq 10^6$ GeV^2; $10^{-6} < x < 1$**

EPS09 **Available so far for only $A =$Au and Pb, more to come; LO and NLO sets available based on CTEQ61L and CTEQ6M respectively; χ^2 analysis done at both LO and NLO; calling routine similar to other sets but now there are 31, 15 above and 15 below the central set; no longer use BRAHMS data**

In all cases, when A, x or Q^2 are outside the range of validity, the last value is returned, *e.g.* if $x < 10^{-6}$ value at $x = 10^{-6}$ is given

EPS09 Fitting Procedure

Define a local χ^2 based on N data sets and a given input parameter set to be varied, $\{a\}$, χ^2_N Set of weight factors w_N used to amplify the importance of χ^2_N to the fit for sets that have large influence but small relative χ^2

$$\begin{aligned}
\chi^2(\{a\}) &\equiv \sum_N w_N \, \chi^2_N(\{a\}) \\
\chi^2_N(\{a\}) &\equiv \left(\frac{1-f_N}{\sigma_N^{\rm norm}}\right)^2 + \sum_{i \in N} \left[\frac{f_N D_i - T_i(\{a\})}{\sigma_i}\right]^2 ,
\end{aligned}$$

D_i are data points with a σ_i point-to-point uncertainty (statistical and systematic uncertainties added in quadrature), f_N is normalization factor for sets with relative normalization uncertainty $\sigma_N^{\rm norm}$ fixed each iteration by minimizing χ^2_N for each parameter set $\{a\}$, T_i is calculated value to be compared to $f_N D_i$

Weak constraint on low x gluons so to cure unwanted parameter drift into unphysical region with stronger shadowing at small A, cured by

$$1000 \left[\left(y_0^G({\rm He}) - y_0^G({\rm Pb}) \right) - \left(y_0^S({\rm He}) - y_0^S({\rm Pb}) \right) \right]^2 \tag{1}$$

If χ^2-minimized set of parameters, $\{a_0\}$, gives best estimate of nPDFs, work in a basis $\{z\}$ that diagonializes covariance matrix, errors in nPDFs computed within 90% confidence criteria, $\Delta\chi^2 = 50$

Upper and lower uncertainties in any observable X can be computed using the prescription

$$\begin{aligned}
(\Delta X^+)^2 &\approx \sum_k \left[\max\left\{ X(S_k^+) - X(S^0), X(S_k^-) - X(S^0), 0 \right\} \right]^2 \\
(\Delta X^-)^2 &\approx \sum_k \left[\max\left\{ X(S^0) - X(S_k^+), X(S^0) - X(S_k^-), 0 \right\} \right]^2
\end{aligned}$$

x Dependence of EKS98

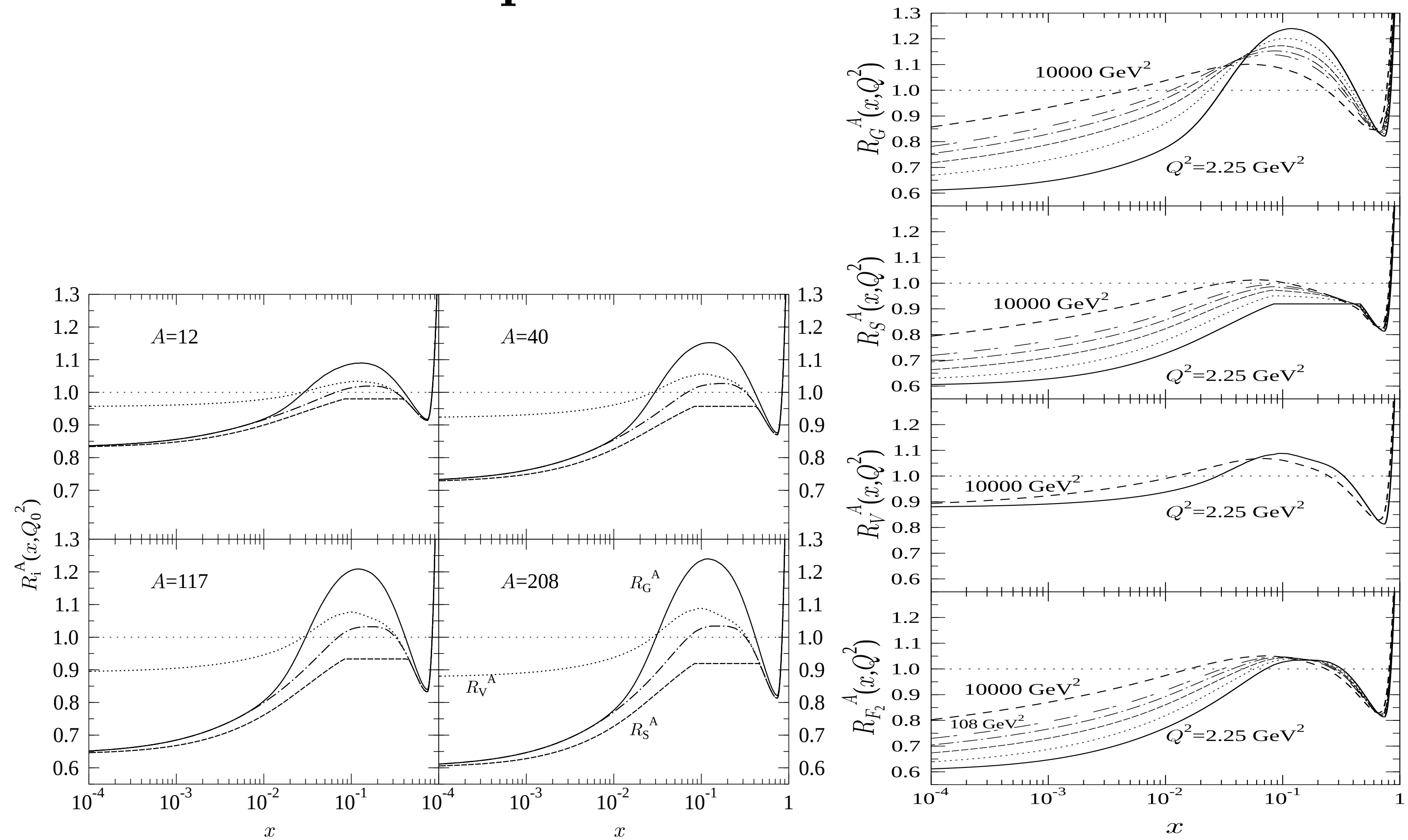

Figure 10: **Left: The initial nuclear ratios R_G^A (solid), R_V^A (dotted), R_S^A (dashed) and $R_{F_2}^A$ (dot-dashed) as a function of x for isoscalar nuclei at $Q_0^2 = 2.25$ GeV^2. Right: Scale evolution of R_G^A (top), R_S^A (second), R_V^A (third) and $R_{F_2}^A$ (bottom) for A =208. The ratios are shown for values equidistant in $\log Q^2$: 2.25 (solid); 5.39 (dotted); 14.7 (close dashed); 39.9 (dot-dashed); 108 (long dashed); and 10000 (dashed) GeV^2. Only the first and last Q^2 values are shown for R_V^A for clarity.**

Q^2 Dependence of EKS98

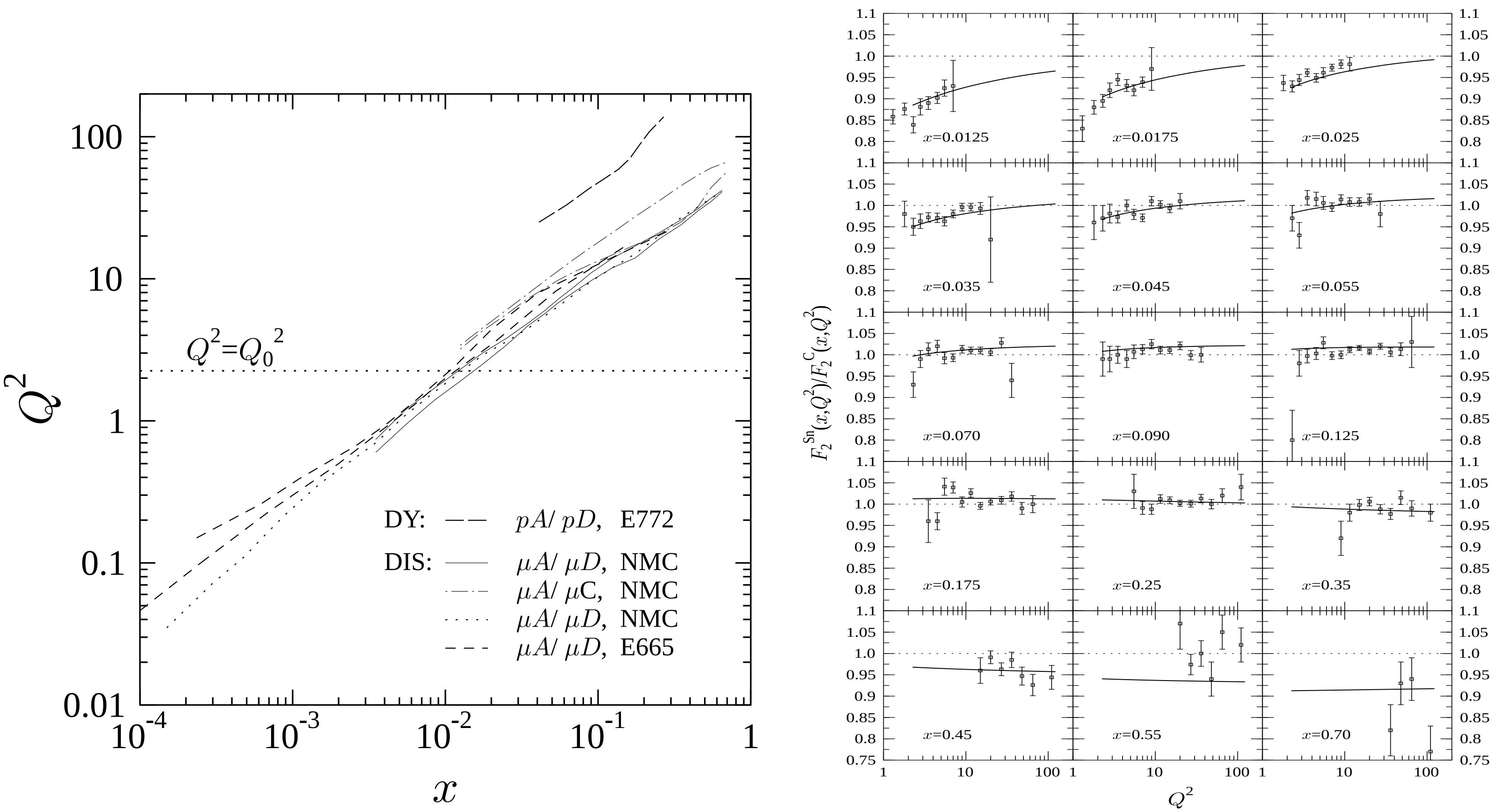

Figure 11: **Left: Correlation of $\langle Q^2\rangle$ and x in nDIS and of invariant mass and $x = x_2$ in pA DY measurements. The horizontal dotted line is the initial scale above which DGLAP evolution is performed. Right: Scale evolution of $F_2^{\mathrm{Sn}}(x,Q^2)/F_2^{\mathrm{C}}(x,Q^2)$ compared with the NMC data. Only statistical uncertainties are shown.**

Data Included in EPS09/EPS08 Fits

EPS09

Experiment	Process	Nuclei	# points	χ^2 LO	χ^2 NLO	Weight
SLAC E-139	DIS	He(4)/D	21	6.5	7.3	1
NMC 95, re.	DIS	He/D	16	14.5	15.6	5
NMC 95	DIS	Li(6)/D	15	23.6	16.8	1
NMC 95, Q^2 dep.	DIS	Li/D	153	162.2	157.0	1
SLAC E-139	DIS	Be(9)/D	20	9.6	12.2	1
NMC 96	DIS	Be/C	15	3.8	3.8	1
SLAC E-139	DIS	C(12)/D	7	4.1	3.2	1
NMC 95	DIS	C/D	15	15.0	13.8	1
NMC 95, Q^2 dep.	DIS	C/D	165	141.8	142.0	1
NMC 95, re.	DIS	C/D	16	19.3	20.5	1
NMC 95, re.	DIS	C/Li	20	30.3	28.4	1
FNAL-E772	DY	C/D	9	7.5	8.3	1
SLAC E-139	DIS	Al(27)/D	20	10.9	12.5	1
NMC 96	DIS	Al/C	15	6.0	5.8	1
SLAC E-139	DIS	Ca(40)/D	7	5.0	4.1	1
FNAL-E772	DY	Ca/D	9	2.9	3.4	15
NMC 95, re.	DIS	Ca/D	15	25.4	24.7	1
NMC 95, re.	DIS	Ca/Li	20	23.9	19.6	1
NMC 96	DIS	Ca/C	15	6.0	6.0	1
SLAC E-139	DIS	Fe(56)/D	26	19.1	23.9	1
FNAL-E772	DY	Fe/D	9	2.1	2.2	15
NMC 96	DIS	Fe/C	15	11.0	10.8	1
FNAL-E866	DY	Fe/Be	28	20.9	21.7	1
CERN EMC	DIS	Cu(64)/D	19	13.4	14.8	1
SLAC E-139	DIS	Ag(108)/D	7	3.8	2.9	1
NMC 96	DIS	Sn(117)/C	15	9.6	9.1	1
NMC 96, Q^2 dep.	DIS	Sn/C	144	80.2	82.8	10 ($x \equiv 0.0125$)
FNAL-E772	DY	W(184)/D	9	7.0	6.7	10
FNAL-E866	DY	W/Be	28	27.3	24.2	1
SLAC E-139	DIS	Au(197)/D	21	11.6	13.8	1
RHIC-PHENIX	π^0 prod.	dAu/pp	20	7.3	6.3	20
NMC 96	DIS	Pb/C	15	6.90	7.2	1
Total			929	738.6	731.3	

EPS08

Experiment	Process	Nuclei	# points	χ^2	Weight
SLAC E-139	DIS	He(4)/D	18	2.0	1
NMC 95, re.	DIS	He/D	16	12.1	1
NMC 95	DIS	Li(6)/D	15	30.7	1
SLAC E-139	DIS	Be(9)/D	17	5.5	1
NMC 96	DIS	Be/C	15	4.2	1
SLAC E-139	DIS	C(12)/D	7	3.5	1
NMC 95	DIS	C/D	15	10.5	5
NMC 95, re.	DIS	C/D	16	17.8	5
NMC 95, re.	DIS	C/Li	20	36.4	1
FNAL-E772	DY	C/D	9	8.9	10
SLAC E-139	DIS	Al(27)/D	17	3.6	1
NMC 96	DIS	Al/C	15	6.7	1
SLAC E-139	DIS	Ca(40)/D	7	1.3	1
FNAL-E772	DY	Ca/D	9	5.0	10
NMC 95, re.	DIS	Ca/D	15	27.9	1
NMC 95, re.	DIS	Ca/Li	20	26.1	1
NMC 96	DIS	Ca/C	15	6.3	1
SLAC E-139	DIS	Fe(56)/D	23	16.5	1
FNAL-E772	DY	Fe/D	9	5.0	10
NMC 96	DIS	Fe/C	15	11.9	1
CERN EMC	DIS	Cu(64)/D	19	12.3	1
SLAC E-139	DIS	Ag(108)/D	7	2.3	1
NMC 96	DIS	Sn(117)/C	15	10.9	1
FNAL-E866	DY	Fe/Be	28	21.6	1
NMC 96, Q^2 ($x \leq 0.025$)	DIS	Sn/C	24	9.4	10
NMC 96, Q^2 ($x > 0.025$)	DIS	Sn/C	120	75.2	1
FNAL-E772	DY	W(184)/D	9	10.0	10
FNAL-E866	DY	W/Be	28	26.5	1
SLAC E-139	DIS	Au(197)/D	18	6.1	1
RHIC-BRAHMS	h^- prod.	dAu/pp	6	2.2	40 .
RHIC-PHENIX	π^0 prod.	dAu/pp	35	21.3	1
RHIC-STAR	$\pi^+ + \pi^-$ prod.	dAu/pp	10	3.5	1
NMC 96	DIS	Pb/C	15	5.1	1
Total			627	448	

Table 1: **The data used in the analyses. The mass numbers are indicated in parentheses and the number of data points refers to those falling within our kinematical cuts, $Q^2, M^2 \geq 1.69\,\mathrm{GeV}^2$ for DIS and DY, and $p_T \geq 2\,\mathrm{GeV}$ for hadron production at RHIC. The quoted χ^2 values correspond to the unweighted contributions of each data set at LO and NLO (LO only for EPS08). The weight factors for each data set are also shown.**

Q^2 Dependence of EPS09

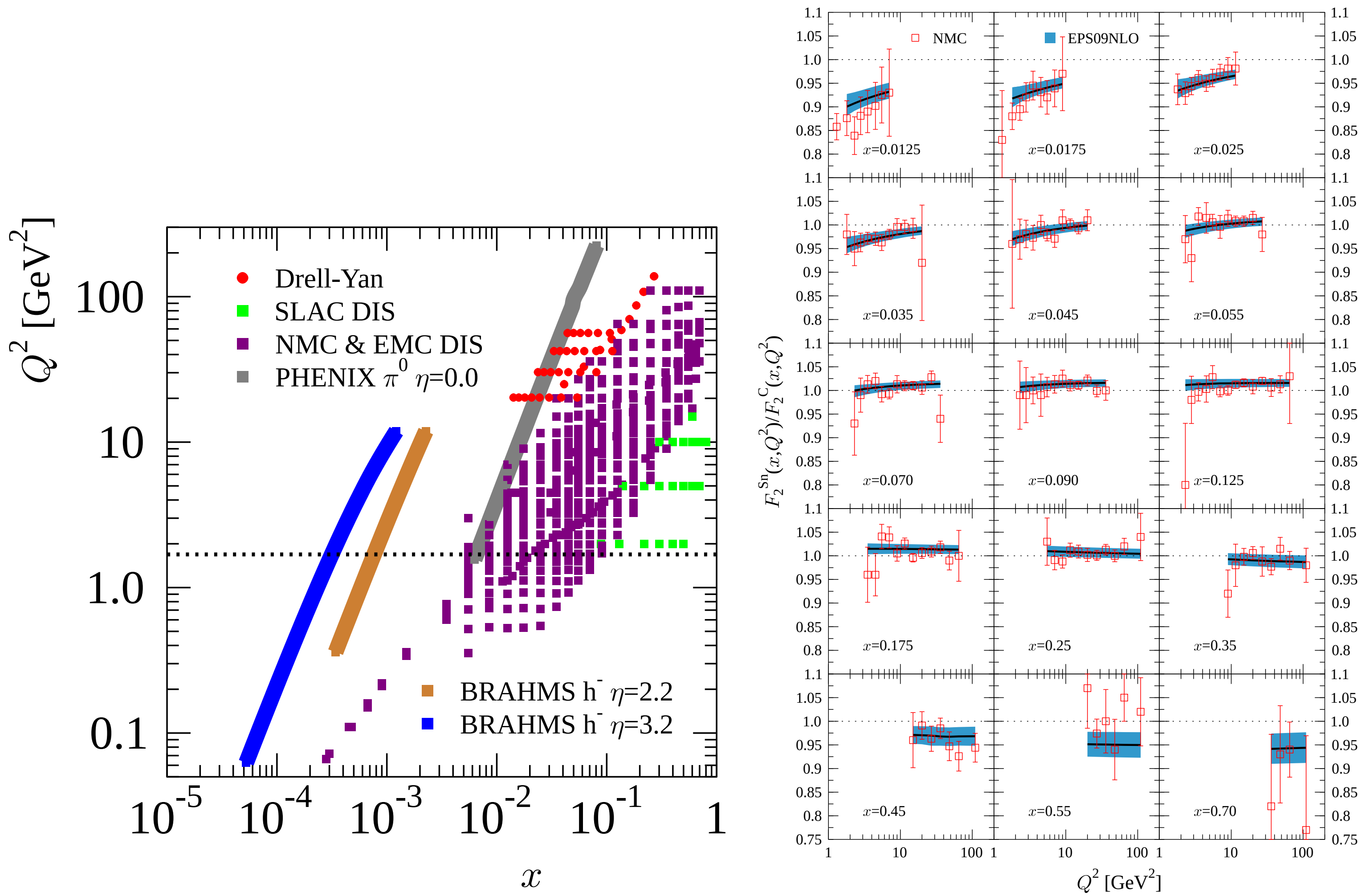

Figure 12: **Left: initial gluon distributions at $Q_0^2 = 1.4$ GeV^2. Right: evolution of gluon distributions for several fixed values of x shows that the effect of the nonlinear terms vanishes as Q^2 increases.**

x Dependence of EPS09 NLO

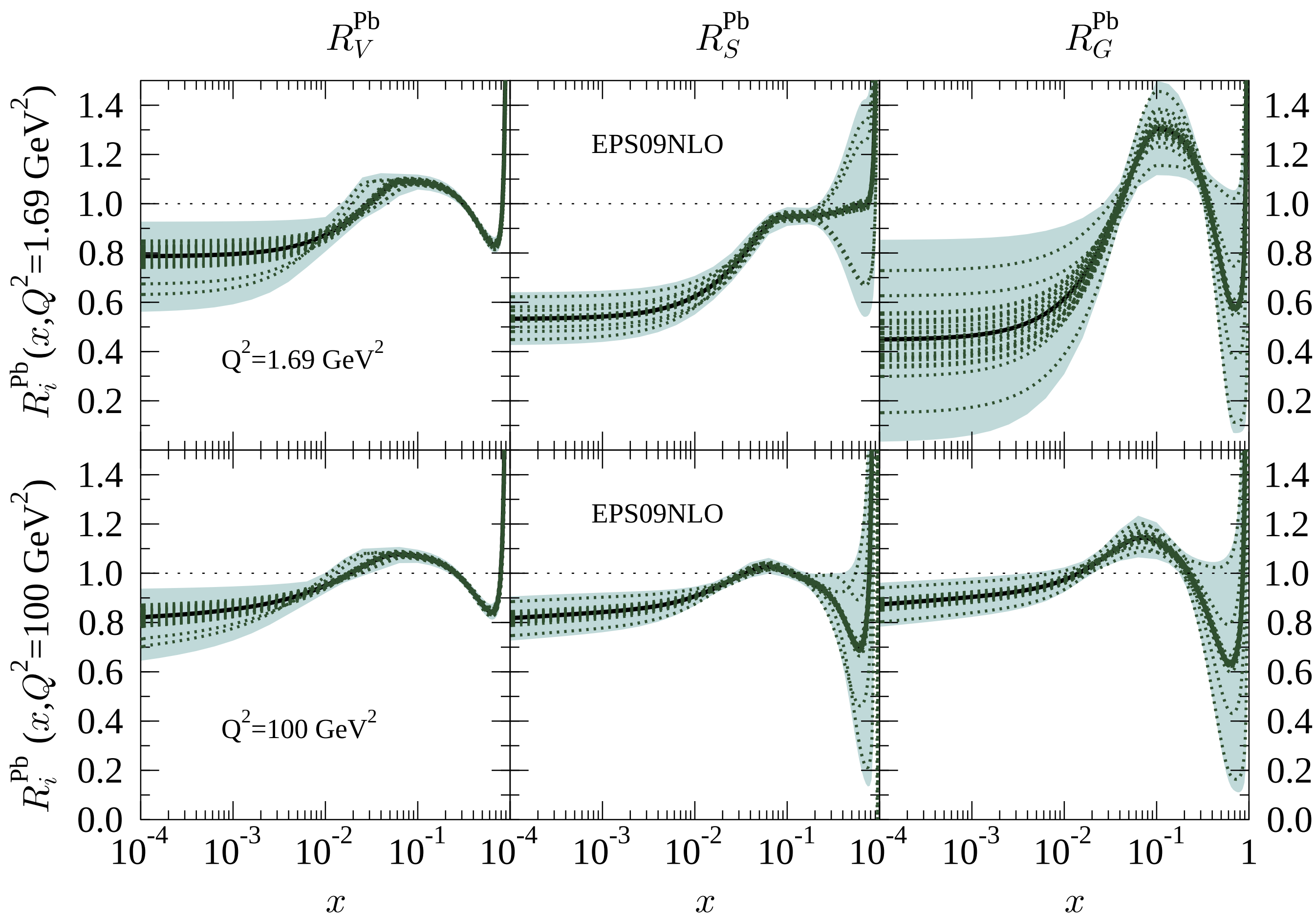

Figure 13: **Left: initial gluon distributions at $Q_0^2 = 1.4$ GeV^2. Right: evolution of gluon distributions for several fixed values of x shows that the effect of the nonlinear terms vanishes as Q^2 increases.**

nDS Sets

Rather than assuming multiplicative ratios only, $f_i^A(x,Q^2) = R_i^A(x,Q^2) f_i(x,Q^2)$, deFlorian and Sassot relate nPDFs to proton PDFs by the convolution

$$f_i^A(x,Q^2) = \int_x^A \frac{dy}{y} W_i(y,A) f_i\Big(\frac{x}{y}, Q_0^2\Big)$$

Neglecting nuclear effects, $W_i(y,A) = A\delta(1-y)$; x shifts in nucleons relative to protons, $W_i(y,A) = A\delta(1-y-\epsilon)$, can describe some features of nPDFs

Evolution done in Mellin space where moments of the nPDFs are equal to the Mellin-space weight factors multiplied by the proton PDF (in this case GRV98)

Charge, baryon number and momentum conservation used as constraints

Even though convolution used in obtaining nPDFs, in practice the nDS code outputs ratios like EKS, EPS

LO and NLO analyses; nDS and nDSg (strong shadowing) sets at each order; $4 < A < 208$; $10^{-6} < x < 1$; $1 < Q^2 < 10^6$ GeV^2

$$\begin{aligned}
W_v(y,A,Z) &= A\,[a_v\,\delta(1-\epsilon_v-y) + (1-a_v)\,\delta(1-\epsilon_{v'}-y)] + n_v\left(\frac{y}{A}\right)^{\alpha_v}\left(1-\frac{y}{A}\right)^{\beta_v} + n_s\left(\frac{y}{A}\right)^{\alpha_s}\left(1-\frac{y}{A}\right)^{\beta_s} \\
W_s(y,A,Z) &= A\,\delta(1-y) + \frac{a_s}{N_s}\left(\frac{y}{A}\right)^{\alpha_s}\left(1-\frac{y}{A}\right)^{\beta_s} \\
W_g(y,A,Z) &= A\,\delta(1-y) + \frac{a_g}{N_g}\left(\frac{y}{A}\right)^{\alpha_g}\left(1-\frac{y}{A}\right)^{\beta_g} \\
\epsilon_i &= \gamma_i + \lambda_i A^{\delta_i} \quad A\,\textbf{dependence of parameters}
\end{aligned}$$

Data Included in nDS Fits

Measurement	Collaboration	# data
F_2^{He}/F_2^D	NMC	18
	SLAC-E139	18
F_2^{Be}/F_2^D	SLAC-E139	17
F_2^C/F_2^D	NMC	18
	SLAC-E139	7
F_2^{Al}/F_2^D	SLAC-E139	17
F_2^{Ca}/F_2^D	NMC	18
	SLAC-E139	7
F_2^{Fe}/F_2^D	SLAC-E139	23
F_2^{Ag}/F_2^D	SLAC-E139	7
F_2^{Au}/F_2^D	SLAC-E139	18
F_2^{Be}/F_2^C	NMC	15
F_2^{Al}/F_2^C	NMC	15
F_2^{Ca}/F_2^C	NMC	15
F_2^{Fe}/F_2^C	NMC	15
F_2^{Pb}/F_2^C	NMC	15
F_2^{Sn}/F_2^C	NMC	145
$\sigma_{DY}^C/\sigma_{DY}^D$	E772	9
$\sigma_{DY}^{Ca}/\sigma_{DY}^D$	E772	9
$\sigma_{DY}^{Fe}/\sigma_{DY}^D$	E772	9
$\sigma_{DY}^W/\sigma_{DY}^D$	E772	9
Total		420

Table 2: **Nuclear data included in the nDS fit.**

x and Q^2 Dependence of nDS

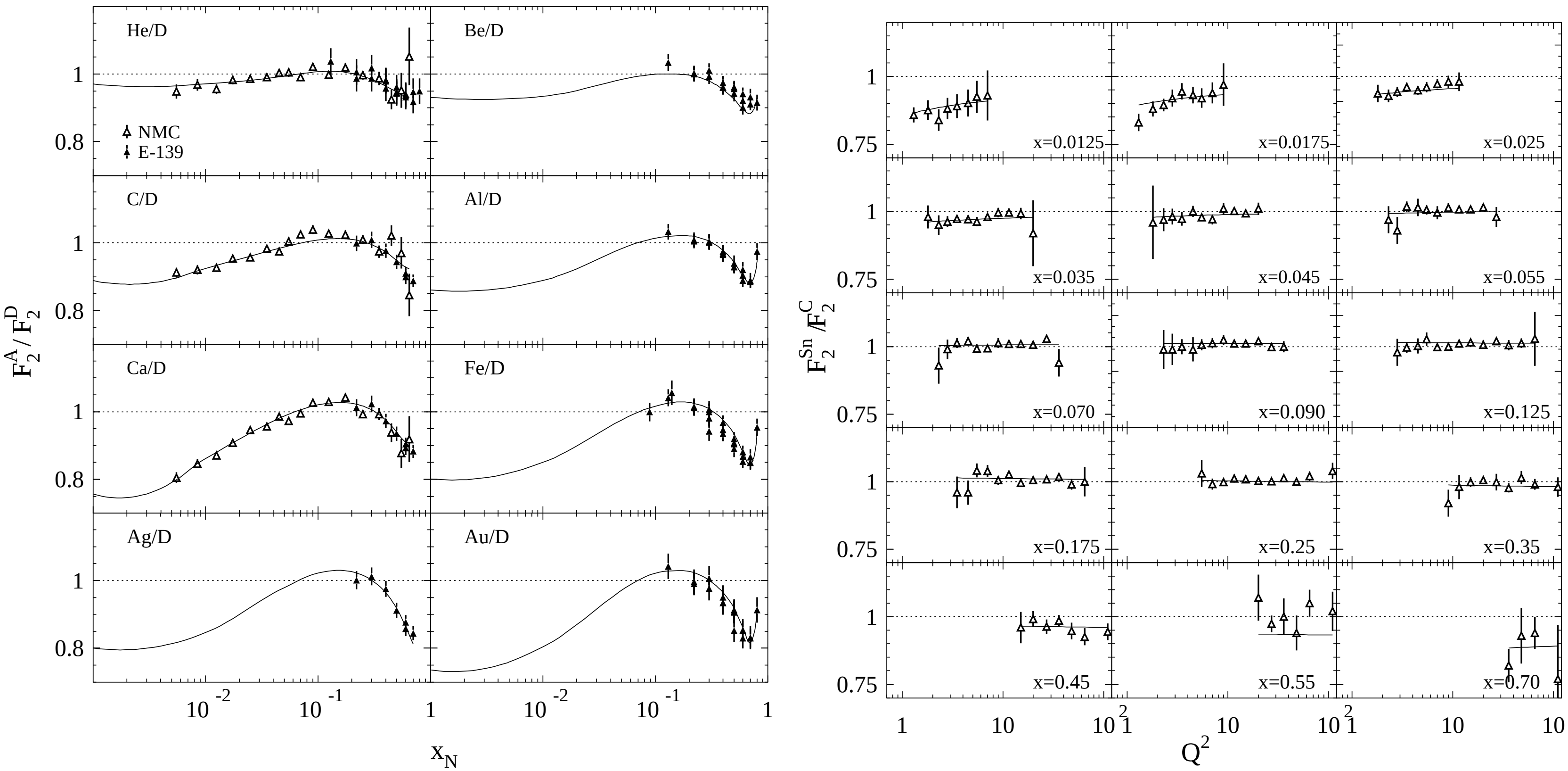

Figure 14: **Left: Structure function ratios F_2^A/F_2^{D} compared to the NLO nDS set. The lines are calculated at the Q^2 of the data. Below the x of the lowest data point, the calculations are extrapolated to low x with the Q^2 of the last measured point. Right: The scale dependence of $F_2^{\mathrm{Sn}}/F_2^{\mathrm{C}}$ at NLO with nDS.**

Comparison of LO and NLO nDS nPDFs

The LO and NLO nuclear modifications for π^0 production are in agreement, as they should be

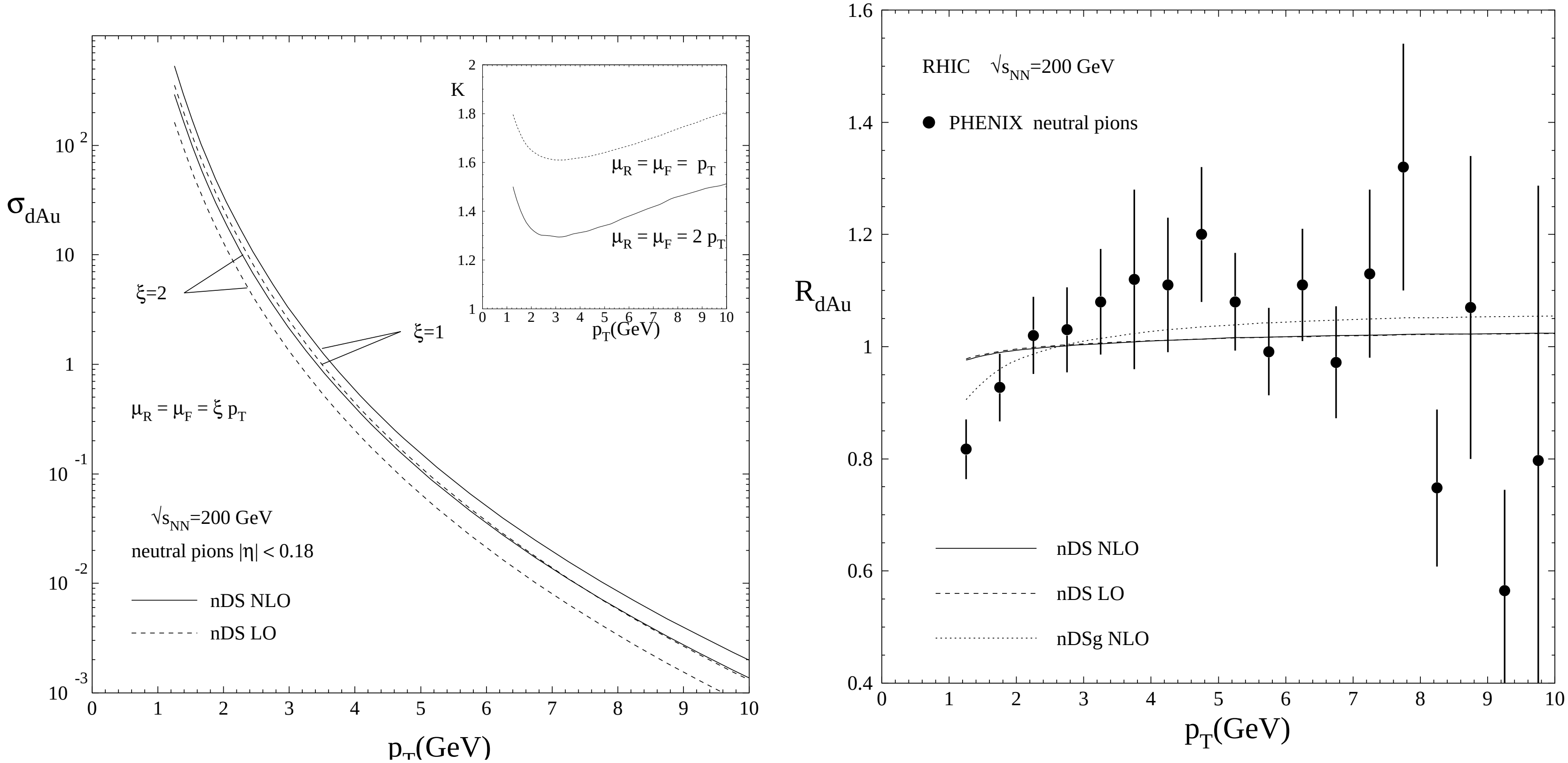

Figure 15: **Left: The π^0 cross section in d+Au collisions at $\sqrt{s_{NN}} = 200$ GeV at LO and NLO. Right: The LO and NLO calculations of R_{dAu}.**

DSSZ Sets

Global fits based on low initial starting scale of $Q_0^2 = 1$ GeV^2, use MSTW set for the free proton baseline

Incorporate charged current νA scattering

Assumes equal modification for valence u and d quarks as well as $\overline{u} = \overline{d} = \overline{s}$ at Q_0^2, evolved separately according to DGLAP afterwards

$$
\begin{aligned}
R_v^A(x, Q_0^2) &= \epsilon_1 x^{\alpha_v}(1-x)^{\beta_1}(1+\epsilon_2(1-x)^{\beta_2})(1+a_v(1-x)^{\beta_3}) \\
R_s^A(x, Q_0^2) &= R_v^A(x, Q_0^2)\frac{\epsilon_s}{\epsilon_1}\frac{1+a_s x^{\alpha_s}}{1+a_s} \\
R_g^A(x, Q_0^2) &= R_v^A(x, Q_0^2)\frac{\epsilon_g}{\epsilon_1}\frac{1+a_g x^{\alpha_g}}{1+a_g}
\end{aligned}
\qquad (2)
$$

Parameters ϵ_1 and ϵ_2 are fixed from charge conservation while ϵ_s is fixed by momentum conservation

A dependence of remaining parameters, $\xi \in \{\alpha_v, \alpha_s, \alpha_g, \beta_1, \beta_2, \beta_3, a_v, a_s, a_g\}$, is given as $\xi = \gamma_\xi + \lambda_\xi A^{\delta_\xi}$, resulting in 25 free fit parameters

Stronger shadowing for sea quarks than gluons, no antishadowing except for valence quarks

Data Included in Obtaining DSSZ Sets

measurement	collaboration .	# points	χ^2	measurement	collaboration .	# points	χ^2
F_2^{He}/F_2^D	NMC	17	18.18	F_2^{Ca}/F_2^C	NMC	15	7.71
	E139	18	2.71	F_2^{Ca}/F_2^C	NMC	24	26.09
F_2^{Li}/F_2^D	NMC	17	17.35	F_2^{Fe}/F_2^C	NMC	15	10.38
F_2^{Li}/F_2^D Q^2 dep.	NMC	179	197.36	F_2^{Sn}/F_2^C	NMC	15	4.69
F_2^{Be}/F_2^D	E139	17	44.17	F_2^{Sn}/F_2^C Q^2 dep.	NMC	145	102.31
F_2^C/F_2^D	NMC	17	27.85	F_2^{Pb}/F_2^C	NMC	15	9.57
	E139	7	9.66	$F_2^{\nu Fe}$	NuTeV	78	109.65
	EMC	9	6.41	$F_3^{\nu Fe}$	NuTeV	75	79.78
F_2^C/F_2^D Q^2 dep.	NMC	191	201.63	$F_2^{\nu Fe}$	CDHSW	120	108.20
F_2^{Al}/F_2^D	E139	17	13.22	$F_3^{\nu Fe}$	CDHSW	133	90.57
F_2^{Ca}/F_2^D	NMC	16	18.60	$F_2^{\nu Pb}$	CHORUS	63	20.42
	E139	7	12.13	$F_3^{\nu Pb}$	CHORUS	63	79.58
F_2^{Cu}/F_2^D	EMC	19	18.62	$d\sigma_{DY}^{C}/d\sigma_{DY}^{D}$	E772	9	9.87
F_2^{Fe}/F_2^D	E139	23	34.95	$d\sigma_{DY}^{Ca}/d\sigma_{DY}^{D}$	E772	9	5.38
F_2^{Ag}/F_2^D	E139	7	9.71	$d\sigma_{DY}^{Fe}/d\sigma_{DY}^{D}$	E772	9	9.77
F_2^{Sn}/F_2^D	EMC	8	16.59	$d\sigma_{DY}^{W}/d\sigma_{DY}^{D}$	E772	9	19.29
F_2^{Au}/F_2^D	E139	18	10.46	$d\sigma_{DY}^{Fe}/d\sigma_{DY}^{Be}$	E866	28	20.34
F_2^C/F_2^{Li}	NMC	24	33.17	$d\sigma_{DY}^{W}/d\sigma_{DY}^{Be}$	E866	28	26.07
F_2^{Ca}/F_2^{Li}	NMC	24	25.31	$d\sigma_{\pi^0}^{dAu}/d\sigma_{\pi^0}^{pp}$	PHENIX	20	27.71
F_2^{Be}/F_2^C	NMC	15	11.76	$d\sigma_{\pi^0}^{dAu}/d\sigma_{\pi^0}^{pp}$	STAR	11	3.92
F_2^{Al}/F_2^C	NMC	15	6.93 $d\sigma_{\pi^\pm}^{dAu}/d\sigma_{\pi^\pm}^{pp}$	STAR	30	36.63	
				Total		1579	1544.70

Table 3: Total and individual χ^2 values for the data sets included in the fit.

x Dependence of DSSZ at Q_0^2

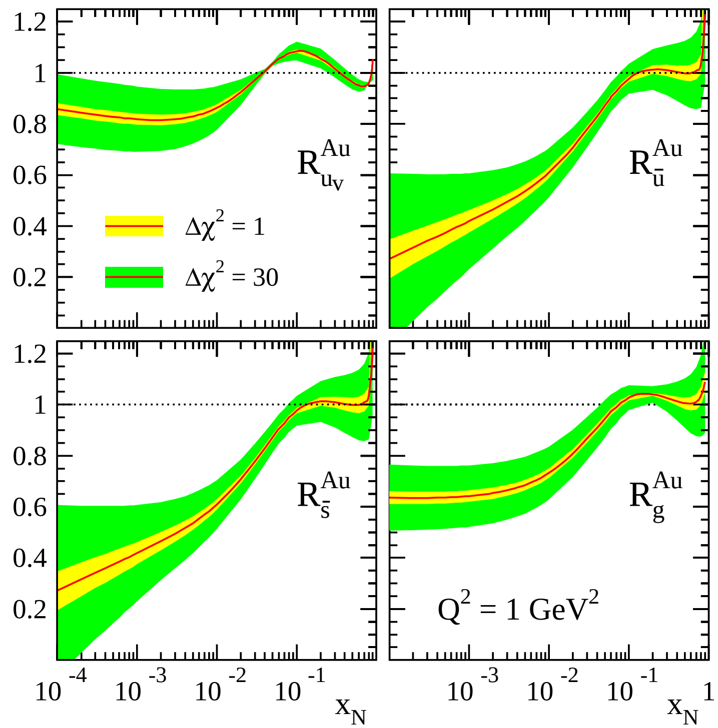

Figure 16: **NLO DSSZ modifications at the starting scale $Q_0^2 = 1$ GeV^2 for a gold nucleus. The inner and outer uncertainty bands correspond to uncertainty estimates for $\Delta\chi^2 = 1$ and 30.**

Q^2 and flavor Dependence of DSSZ

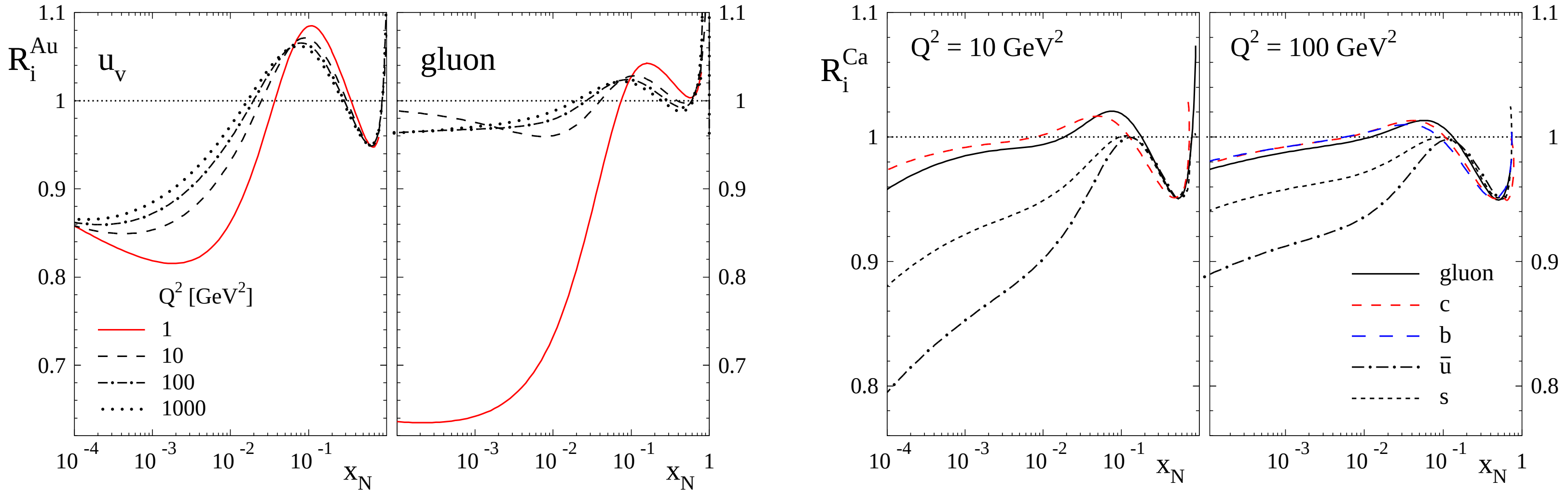

Figure 17: **Left: Scale dependence of the valence quark and gluon ratios for Au. Right: Comparison of nuclear modifications in Ca for $\overline{u}$, $\overline{s}$, c, b and g for two different values of Q^2.**

HKN Sets

Fits weight functions for ratios $f_i^A(x,Q_0^2) = w_i(x,A,Z) f_i(x,Q_0^2)$**,**
Relate nPDFs to proton PDFs by the convolution

$$w_i(x,A,Z) = 1 + \left(1 - \frac{1}{A^\alpha}\right) \frac{a_i(A,Z) + b_i x + c_i x^2 + d_i x^3}{(1-x)^{\beta_i}}$$

LO analysis; based on MRST01-LO PDFs; Hessian (covariance) method used to determine uncertainties on the nPDFs; $10^{-9} < x < 1$**;** $1 < Q^2 < 10^8$ **GeV**^{2}

HKN requires both Z **and** A

$$\begin{aligned}
u_v^A(x,Q_0^2) &= w_{u_v}(x,A,Z)\,\frac{Z u_v(x,Q_0^2) + N d_v(x,Q_0^2)}{A}, \\
d_v^A(x,Q_0^2) &= w_{d_v}(x,A,Z)\,\frac{Z d_v(x,Q_0^2) + N u_v(x,Q_0^2)}{A}, \\
\bar{q}^A(x,Q_0^2) &= w_{\bar{q}}(x,A,Z)\,\bar{q}(x,Q_0^2), \\
g^A(x,Q_0^2) &= w_g(x,A,Z)\,g(x,Q_0^2)
\end{aligned}$$

Available for limited set of nuclei:

Nucleus	A	Z	Nucleus	A	Z
p	1	1	Fe	56	26
d	2	1	Cu	63	29
He	4	2	Kr	84	36
Li	7	3	Ag	107	47
Be	9	4	Sn	118	50
C	12	6	Xe	131	54
N	14	7	W	184	74
Al	27	13	Au	197	79
Ca	40	20	Pb	208	82

Table 4: **Available nuclei for the HKN parameterization.**

Data Included in HKN Fits

Measurement	Collaboration	# points
	F_2^A/F_2^D	
^{4}He/D	SLAC-E139	18
	NMC-95	17
Li/D	NMC-95	17
Be/D	SLAC-E139	17
C/D	EMC-88	9
	EMC-90	5
	SLAC-E139	7
	NMC-95	17
	FNAL-E665-95	5
N/D	BCDMS-85	9
	HERMES-03	153
Al/D	SLAC-E49	18
	SLAC-E139	17
Ca/D	EMC-90	5
	NMC-95	16
	SLAC-E139	7
	FNAL-E665-95	5
Fe/D	SLAC-E87	14
	SLAC-E140	10
	SLAC-E139	23
	BCDMS-87	10
Cu/D	EMC-93	19
Kr/D	HERMES-03	144
Ag/D	SLAC-E139	7
Sn/D	EMC-88	8
Xe/D	FNAL-E665-92	5
Au/D	SLAC-E140	1
	SLAC-E139	18
Pb/D	FNAL-E665-95	5
F_2^A/F_2^D total		606

Measurement	Collaboration	# points
	$F_2^A/F_2^{A'}$	
Be/C	NMC-96	15
Al/C	NMC-96	15
Ca/C	NMC-95	24
	NMC-96	15
Fe/C	NMC-96	15
Sn/C	NMC-96	146
Pb/C	NMC-96	15
C/Li	NMC-95	24
Ca/Li	NMC-95	24
$F_2^A/F_2^{A'}$ total		293
	$\sigma_{DY}^{pA}/\sigma_{DY}^{pA'}$	
C/D	FNAL-E772-90	9
Ca/D	FNAL-E772-90	9
C/Li	NMC-95	24
W/D	FNAL-E772-90	9
Fe/Be	FNAL-E866/NuSea-99	8
W/Be	FNAL-E866/NuSea-99	8
Drell-Yan total		52
Total		951

Table 5: **Nuclear data included in the nDS fit.**

Q^2 Dependence of HKN

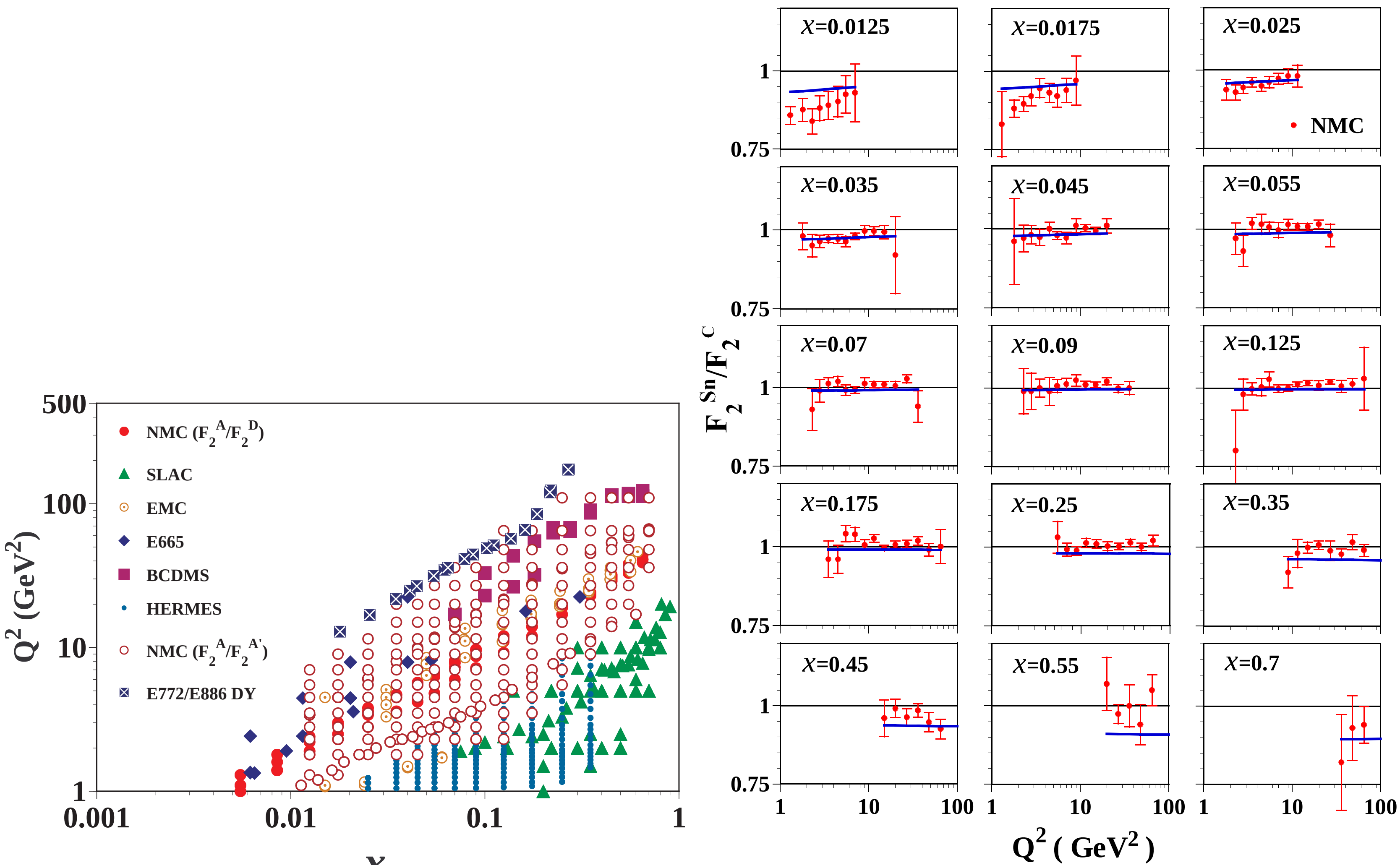

Figure 18: **Left: The kinematic range of the fits in x and Q^2. Right: The scale evolution of $F_2^{\rm Sn}/F_2^{\rm C}$.**

x Dependence of HKN

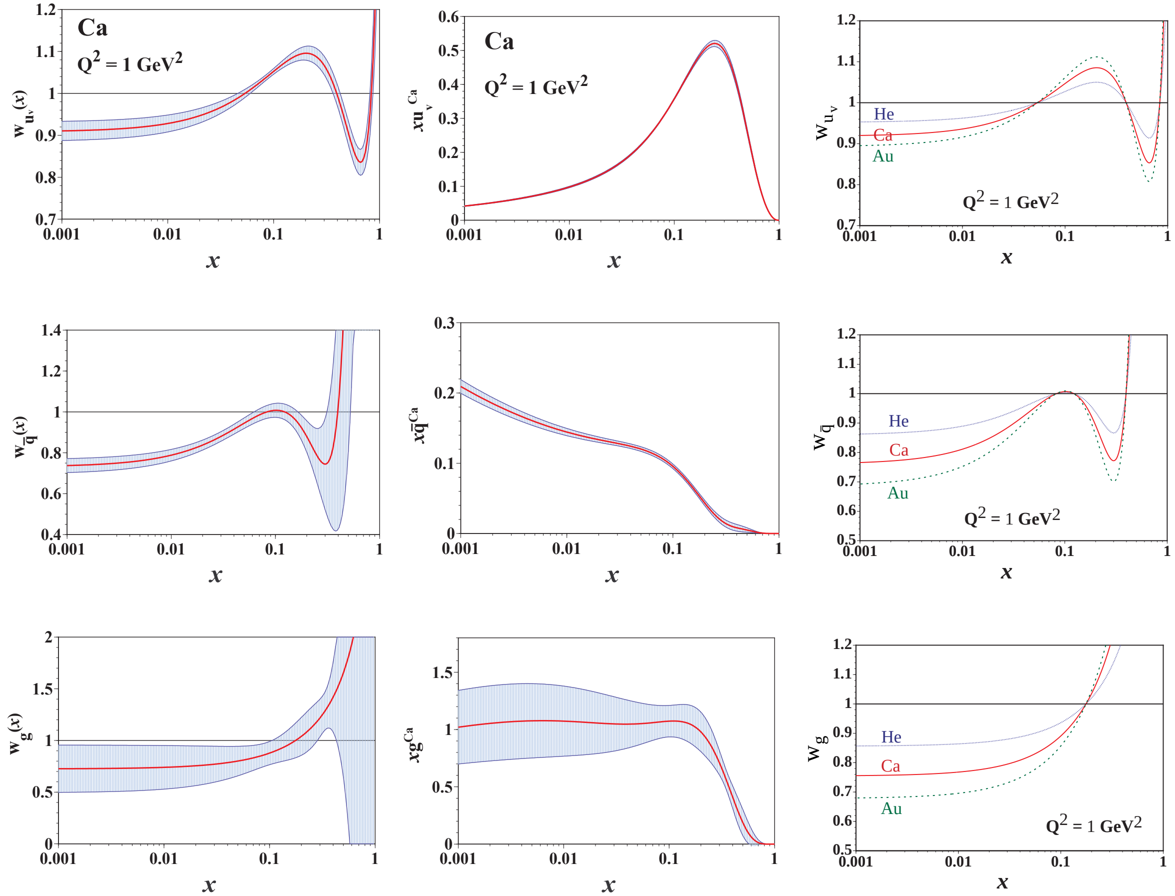

Figure 19: **The weight functions (left) and the nuclear parton distribution functions (middle) are shown for A =Ca at Q_0^2. The uncertainties are shown by the bands. The A dependence of the weight functions (shadowing ratios) are shown for A =He, Ca and Au at $Q^2 = 1$ GeV^2.**

FGS10

NLO predictions for leading-twist shadowing based on diffraction in ep DIS, experimental uncertainty due to uncertainty on t dependence of the proton diffractive structure functions

Since the inclusive and diffractive structure functions are obtained from the convolution of the corresponding parton densities with the same hard scattering coefficients, three is a relation between the nuclear parton densities, $xf_{j/A}$, and the diffractive nucleon parton densities, $f_j^{D(4)}$, derived from scattering with two target nucleons,

$$
\begin{aligned}
xf_{j/A}^{(b)}(x,Q^2) &= -8\pi A(A-1)\Re e\frac{(1-i\eta)^2}{1+\eta^2}\int_x^{0.1} dx_{I\!P}\beta f_j^{D(4)}(\beta,Q^2,x_{I\!P},t_{\min}) \\
&\times \int d^2\vec{b}\int_{-\infty}^{\infty} dz_1 \int_{z_1}^{\infty} dz_2\, \rho_A(\vec{b},z_1)\rho_A(\vec{b},z_2)e^{i(z_1-z_2)x_{I\!P}m_N} .
\end{aligned}
$$

Obtained two sets of nPDFs based on strong (H) or weaker (L) shadowing with minimum scale $Q_0^2 = 4$ GeV^2 and x range $x \leq 10^{-4}$, evolution based on DGLAP

H set: gluon is well approximated by the black disk regime; sizeable color fluctuations for the quarks, modeled by a coefficient that depends on averages over powers of the dipole $q\overline{q}-N$ cross section

L set: based on πN scattering cross section through moments of the distribution $P_j(\sigma)$ determined from the interactions of k target nucleons, $\langle\sigma^k\rangle_j = \int d\sigma P_j(\sigma)\sigma^k$, accounts for color fluctuations; this approach is independent of flavor at low x

x Dependence of FGS

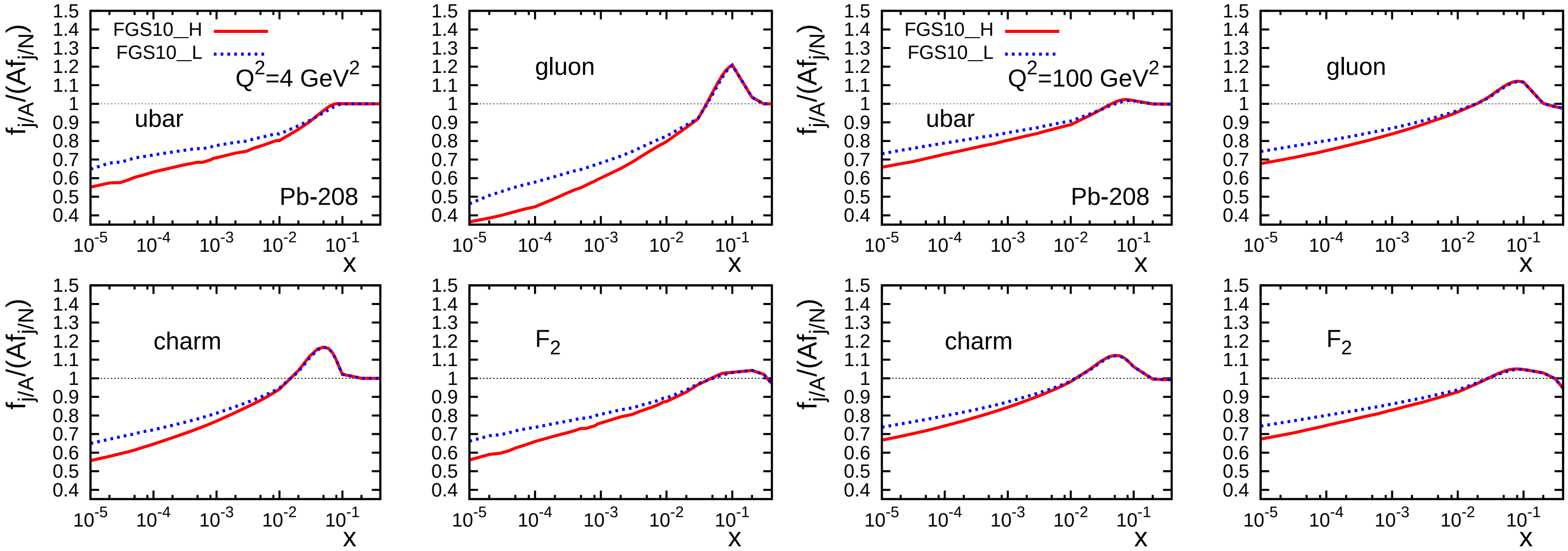

Figure 20: **The NLO ratio of nuclear to proton PDFs in Pb calculated at $Q^2 = 4$ GeV^2 (left) and 100 GeV^2 (right).**

Q^2 Dependence of FGS10

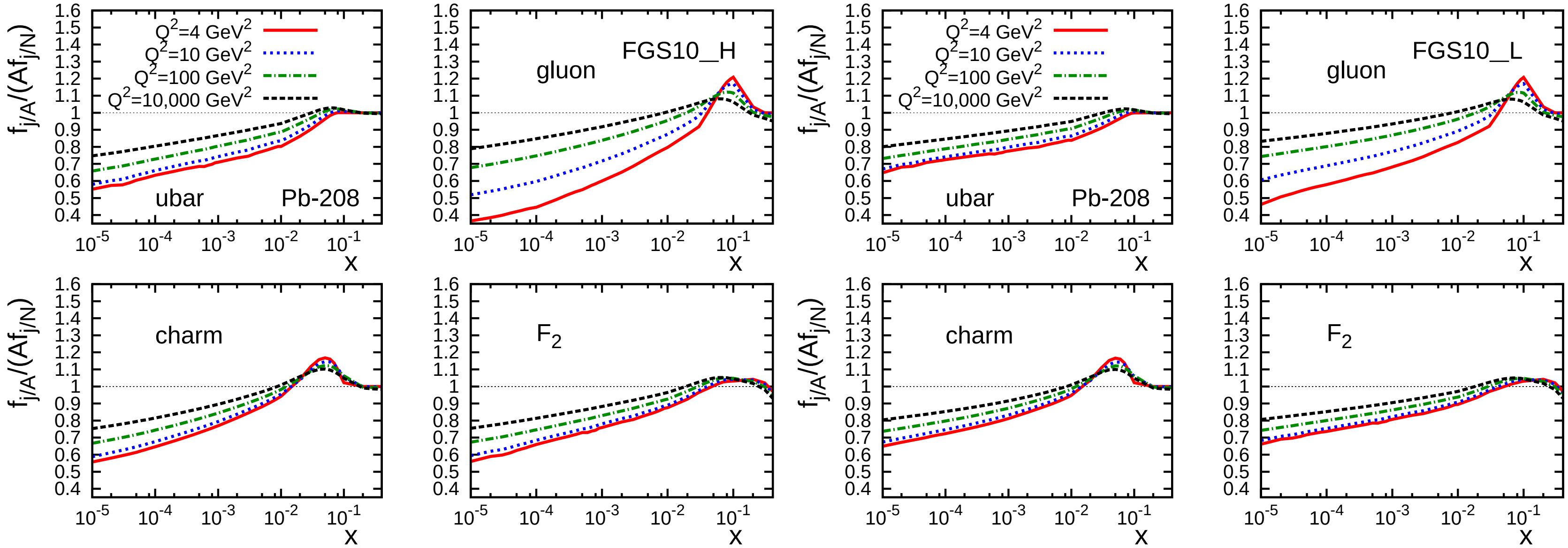

Figure 21: **Ratio of nuclear to proton NLO parton distributions in Pb calculated at $Q^2 = 4$ (solid red); 10 (dotted blue); 100 (dot-dashed green) and 10000 (dashed black) GeV^2 for FGS10_H (left) and FSG10_L (right).**

A Dependence of FGS10

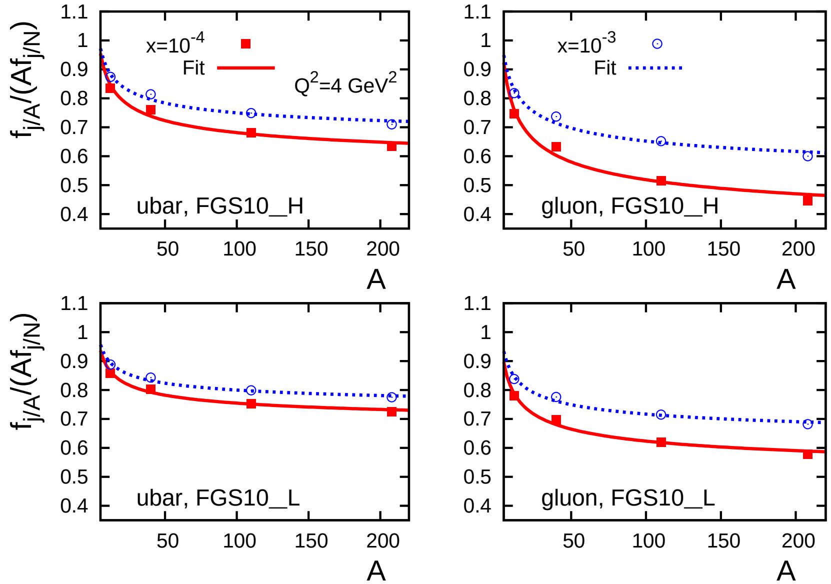

Figure 22: **Ratio of nuclear to proton NLO parton distributions as a function of nuclear mass A for $x = 10^{-4}$ (solid red) and 10^{-3} (dotted blue) for FGS10_H and FGS10_L. The smooth curves are two-parameter fits.**

Centrality Dependence of Nuclear Modifications

Impact Parameter Dependence of FGS10

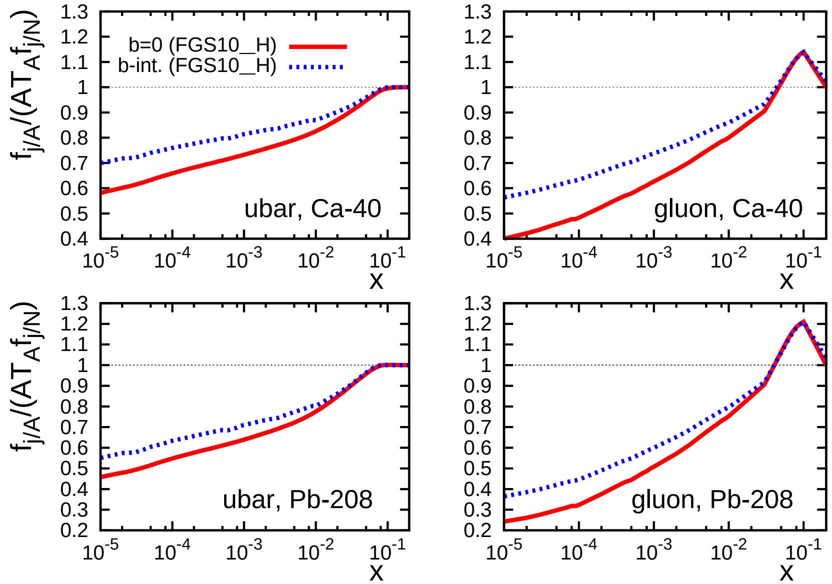

Figure 23: **The difference between the FGS10_H ratios at $b = 0$ (solid red) and integrated over impact parameter (dashed blue) for Ca (top) and Pb (bottom).**

Impact Parameter Dependence of EPS09s

Previous impact-parameter dependent EPS09 calculations were based on linear dependence on nuclear profile function $T_A(s)$

EPS09s (and EKS98s) sum up to quadratic terms in $T_A(s)$ to get A independent coefficients
Result is somewhat similar to dependence of FGS10

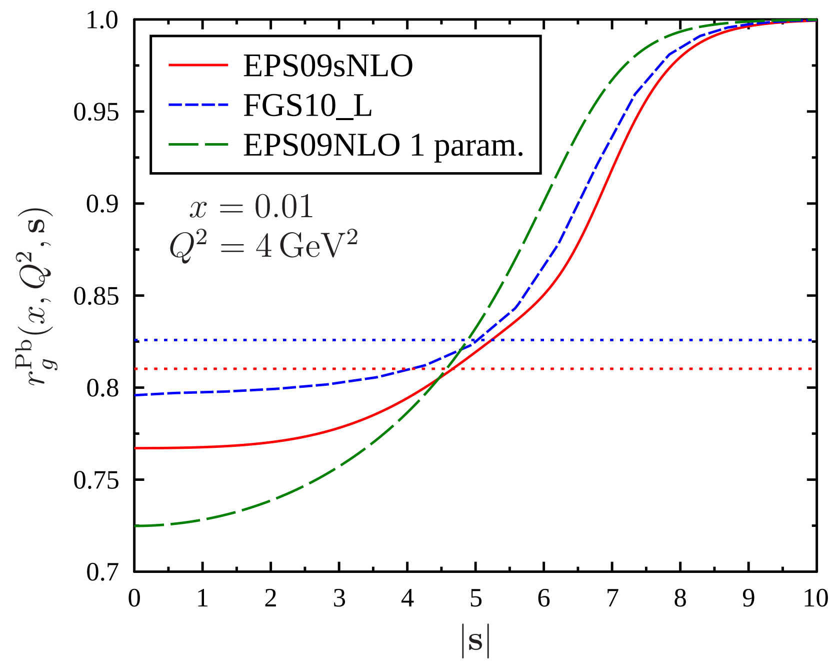

Figure 24: **Comparison of the spatial dependence of the gluon modification in a lead nucleus, $r_g^{\mathrm{Pb}}(x, Q^2, s)$, between FGS10_L (short-dashed blue curves), 1-parameter approach (long-dashed green) and our spatial fits (solid red) EPS09sNLO1. The scale $Q^2 = 4$ GeV^2 for all plots but the values of x have been chosen so that the spatially averaged $R_g^{\mathrm{Pb}}(x, Q^2)$ (dotted horizontal red lines) approximately coincides with FGS10_L (dotted blue).**